JOURNAL OF Materials CHEMISTRY

Synthesis and characterization of PtRu/C catalysts from microemulsions and emulsions

Zhaolin Liu,*[a] Jim Yang Lee,[b,c] Ming Han,[a] Weixiang Chen[c] and Leong Ming Gan[a]

[a]*Institute of Materials Research & Engineering, 3 Research Link, Singapore 117602. E-mail: zl-liu@imre.org.sg*
[b]*Department of Chemical and Environmental Engineering, National University of Singapore, 10 Kent Ridge Crescent, Singapore 119260*
[c]*Singapore–MIT Alliance (SMA), National University of Singapore, 10 Kent Ridge Crescent, Singapore 119260*

Received 23rd January 2002, Accepted 15th April 2002
First published as an Advance Article on the web 7th June 2002

Nanosized PtRu catalysts supported on carbon have been synthesized from inverse microemulsions and emulsions using H_2PtCl_6 (0.025 M)/$RuCl_3$ (0.025 M)/NaOH (0.025 M) as the aqueous phase, cyclohexane as the oil phase, and NP5 (poly(oxyethylene)$_5$ nonyl phenol ether) or NP9 (poly(oxyethylene)$_9$ nonyl phenol) as the surfactant, in the presence of Carbon Black suspended in a mixture of cyclohexane and NP5 + NP9. The titration of 10% HCHO aqueous solution into the inverse microemulsions and emulsions resulted in PtRu/C catalysts, in which the PtRu particles were nanometers in size. The catalysts were characterized by TEM, XRD and XPS and the metal particles were found to inherit the Pt fcc structure with Pt and Ru mostly in the zero valence oxidation states, amidst some Pt(II), Pt(IV) and Ru(IV). The cyclic voltammograms for methanol oxidation on these PtRu/C catalysts showed higher electrocatalytic activities for the two microemulsion derived catalysts than the emulsion-derived electrocatalyst.

Introduction

PtRu alloys are currently the most active anode catalysts for the oxidation of methanol or CO-contaminated H_2, (*e.g.*, H_2 derived from reformed methanol) in low temperature solid polymer electrolyte fuel cells such as the direct methanol fuel cells (DMFC)[1–3] or the indirect methanol fuel cells (IMFC).[4] In the latter, methanol reacts with water to produce a reformate gas with typical composition of 75% H_2, 24% CO_2 and about 1% CO. However, the performance of an IMFC is significantly affected by CO concentrations as low as a few parts per million.[5] This is due to strong adsorption of carbon monoxide on the Pt anode inhibiting the hydrogen oxidation reaction. PtRu alloy electrodes have shown much higher CO tolerance[6] and similar kinetics for H_2 oxidation as Pt electrocatalysts.[7] This is because water dissociation occurs preferentially on the Ru sites; resulting in the formation of Ru–OH groups which may then react with the methanolic residues on neighbouring Pt sites to produce carbon dioxide. Therefore, adsorbed CO is oxidized at potentials more negative than that on Pt. Thus, the Pt surface sites become more available for hydrogen adsorption and oxidation.

High surface area catalysts are generally prepared by co-impregnation,[8] coprecipitation,[9] absorbing alloy colloids[10,11] or surface organometallic chemistry techniques.[12] For both alloy and oxide promoted catalytic systems it is important that Pt and the second metal (or metal oxide) are in intimate contact.[11] This close association of platinum and co-catalysts can be difficult to achieve using conventional catalyst preparation techniques because the active components may be deposited at different sites on the support surface. As the preparation details control the final composition, surface structure and morphology of the catalysts, it is not surprising to find catalytic activities being strongly dependent on the preparation conditions.[13]

The preparation of nano-inorganic particles has been one of the most pursued goals in R&D efforts. However, it is difficult to obtain small particles by classical methods. More advanced approaches (*e.g.* sol–gel processes,[14,15] microemulsion techniques,[16] emulsion polymerizations,[17] and miniemulsion techniques[18]) have been used to produce nanoparticles with the required properties.

A microemulsion is generally defined as a system composed of a mixture of water or brine, hydrocarbon(s) and amphiphilic compound(s) in the form of a thermodynamically stable and optically isotropic solution.[19] The term amphiphiles refers to surfactants as well as co-surfactants, such as a short-chain alcohol. A transparent microemulsion can be formed as droplets of oil-swollen micelles dispersed in water (known as oil-in-water (o/w) microemulsions), or water-swollen micelles dispersed in oil (known as water-in-oil (w/o) microemulsions). Between the o/w and w/o microemulsion regions, there may exist bicontinuous microemulsions, where oil and water domains are randomly interconnected to form sponge-like nanostructures. In any case, the size of nanostructures in microemulsions may range from about 5 to 70 nm. Due to these unique nanosized structures, microemulsion processing is deemed to be a novel method for producing nanostructural materials, such as polymers, inorganic materials and inorganic/polymer nanocomposites.[20]

This report is an account of the preparation and characterization of carbon-supported PtRu electrocatalysts derived from microemulsion techniques.

Experimental

Hydrogen hexachloroplatinate(IV) hydrate from Aldrich, ruthenium(III) chloride and sodium hydroxide from Sigma, formaldehyde solution from BDH, cyclohexane from Fisher Chemicals, nonionic surfactants of poly(oxyethylene)$_5$ nonyl phenol ether (NP5) and poly(oxyethylene)$_9$ nonyl phenol ether (NP9) from Albright & Wilson Asia, were used as received. Water was purified by a Milli-Q water purification system. Carbon Black (Vulcan XC-72, Cabot) with a specific surface

area (BET) of 250 m^2 g^{-1} was used as the support for all catalysts. The single-phase microemulsion region was determined visually by titrating a known amount of cyclohexane and NP5 and NP9 mixture (in weight ratio of 2 : 1) with an aqueous solution containing H_2PtCl_6 (0.025 M)/$RuCl_3$ (0.025 M)/NaOH (0.025 M) in a screw-capped tube. Each titration was thoroughly mixed using a Vortex mixer. The microemulsion, either of the inverse or the bicontinuous type, would appear optically transparent when the size of aqueous droplets or the thickness of aqueous channels was in the range 5–20 nm.[21] This is because nanosized aqueous droplets or channels do not cause a substantial degree of light scattering. A series of such demarcation points were obtained by varying the cyclohexane to surfactant ratio. The clear–turbid boundaries were established from systematic titration. The transparent microemulsion region is represented by the shaded area shown in Fig. 1.

Three compositions (A, B, C) were chosen for the preparation of PtRu/C (Pt 20 wt.%, Ru 20 wt.%) catalyst precursors at room temperature: (A) a transparent microemulsion consisting of a 10 wt.% H_2PtCl_6 (0.025 M)/$RuCl_3$ (0.025 M)/NaOH (0.025 M) aqueous phase, 65 wt.% cyclohexane and 25 wt.% NP5 + NP9 (2 : 1); (B) a translucent liquid consisting of a 30 wt.% H_2PtCl_6 (0.025 M)/$RuCl_3$ (0.025 M)/NaOH (0.025 M) aqueous phase, 50 wt.% cyclohexane and 20 wt.% NP5 + NP9 (2 : 1); (C) a turbid emulsion consisting of a 73 wt.% H_2PtCl_6 (0.025 M)/$RuCl_3$ (0.025 M)/NaOH (0.025 M) aqueous phase, 18 wt.% cyclohexane and 9 wt.% NP5 + NP9 (2 : 1). For the preparation of PtRu/C catalysts, approximately 0.4 g Carbon Black was dispersed and ultrasonicated in a mixture of cyclohexane and NP5 + NP9 for 1 h, followed by the addition of the aqueous solution in amounts corresponding to the overall compositions of A, B and C in the last paragraph. A stoichiometric quantity of 10% HCHO solution was added to each of the three mixtures, under vigorous agitation by magnetic stir bars. The mixtures were then left for 24 h, the catalyst precursors were recovered by filtration and thoroughly washed with distilled ethanol to remove residual oil and surfactants. The three catalyst's precursor's powders were dried under vacuum at approximately 60 °C, before calcination in N_2 at 450 °C for 2 h.

TEM measurements were carried out on a Philips CM 300 FEG system. Samples were first ultrasonicated in acetone for 1 h and then deposited on 3 mm Cu grids covered with continuous carbon films. X-ray photoelectron spectroscopy (XPS) analyses of the samples were performed on a VG ESCALAB MKII spectrometer. Narrow scan photoelectron spectra were recorded for C 1s, O 1s, Ru 3p and Pt 4f. Peak deconvolution was performed using the curve-fitting program VGX900. Powder X-ray diffraction (XRD) was conducted on a Philips PW1877 diffractometer using Cu Kα radiation and a graphite monochromator. An EG&G Model 273 potentiostat/galvanostat, and a conventional three-electrode test cell were used for electrochemical measurements. The working electrode was a thin layer of Nafion-impregnated catalyst cast on a vitreous carbon disk electrode. Pt gauze and a saturated calomel electrode (SCE) were used as the counter and reference electrodes, respectively. All potentials in this report are quoted against the SCE. All electrolyte solutions were deaerated by bubbling high-purity argon for 2 h prior to any measurement. For the hydrogen electrosorption curves, the electrode was activated by cycling the potential between −0.2 and +1.2 V *vs.* SCE at 50 mV s^{-1} in 0.5 M H_2SO_4. The lower and upper potential limits were chosen to be close to H_2 and O_2 evolution potentials, respectively. More than 20 activation scans were needed to obtain reproducible features in the hydrogen electrosorption region. The potential was then swept between +0.25 and −0.25 V at 10 mV s^{-1} to obtain the hydrogen voltammetric profiles in Ar purged electrolytes. For cyclic voltammetry of methanol oxidation, the electrolyte solution was 2 M CH_3OH in 1 M H_2SO_4, which was prepared from high-purity sulfuric acid, high-purity grade methanol and distilled water. No preconditioning was applied in this case.

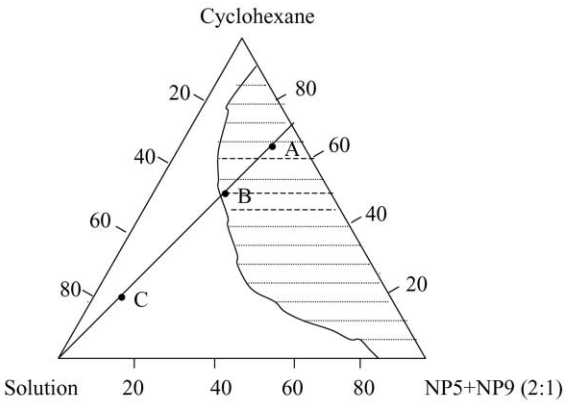

Fig. 1 The partial phase diagram for the system consisting of cyclohexane–(NP5 + NP9)–aqueous solution of H_2PtCl_6 (0.025 M)/$RuCl_3$ (0.025 M)/NaOH (0.025 M) at room temperature.

Results and discussion

Fig. 1 shows the phase diagram for the system cyclohexane–(NP5 + NP9)–aqueous solution of H_2PtCl_6 (0.025 M)/$RuCl_3$ (0.025 M)/NaOH (0.025 M) at room temperature. The microemulsion region is indicated by the shaded area. Any mixture of cyclohexane, surfactant (NP5 + NP9), and aqueous solution within the shaded region is optically clear because the aqueous phase exists as discrete domains too small for light scattering (5–20 nm).[21] From the figure, for a fixed oil to surfactant weight ratio of 70 : 30, the maximum aqueous content for the formation of a microemulsion would be limited to 30 wt.% of 0.025 M H_2PtCl_6/0.025 M $RuCl_3$/0.025 M NaOH. The demarcation between the microemulsion and non-microemulsion regions was determined visual examination of turbid to transparent transitions. Fig. 2 shows the electrical conductivity of the water–oil mixture as a function of the amount of aqueous H_2PtCl_6 (0.025 M)/$RuCl_3$ (0.025 M)/NaOH (0.025 M) introduced at a fixed cyclohexane to surfactant ratio of 7 : 3. The electrical conductivity was very low in the 0–40 wt.% aqueous solution, indicating that the transparent region containing <31 wt.% of the aqueous phase was inverse microemulsions where the conductivity of the aqueous phase is limited to the dispersed droplets in the oil phase. A sudden increase in electrical conductivity is expected to occur when the aqueous channels interconnect to transform the inverse microemulsion

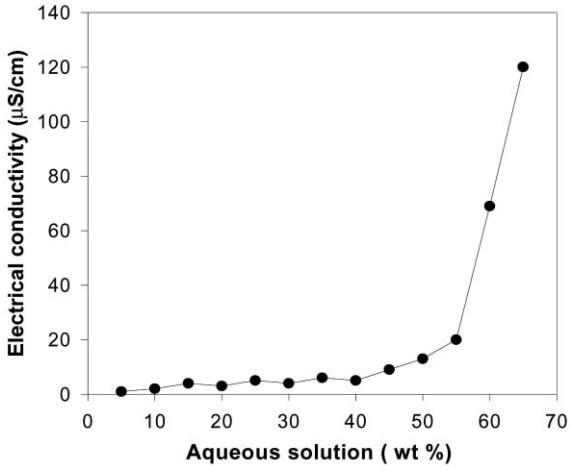

Fig. 2 The electrical conductivity as a function of content of aqueous H_2PtCl_6 (0.025 M)/$RuCl_3$ (0.025 M)/NaOH (0.025 M) in the compositions of fixed cyclohexane to surfactant ratio of 7 : 3.

into a bicontinuous microemulsion.[22] This transition was not observed under the experimental conditions. Instead, the sudden increase in electrical conductivity at aqueous contents >55 wt.% was due to the latter becoming a continuous phase and forming a turbid emulsion. Hence, the chosen compositions of A and C correspond to a transparent (inverse) microemulsion and a turbid emulsion, respectively. The translucent composition B, which is close to the microemulsion/emulsion boundary, was an inverse microemulsion.

Fig. 3(a)–(c) are TEM images depicting the morphology of PtRu/C catalyst precursors from compositions A, B and C, respectively. The PtRu particles obtained from compositions A and B were small spherical particles that were fairly well dispersed, and had a uniform particle size distribution. The spherical particle morphology might be an indirect indication that the redox reaction between H_2PtCl_6 or $RuCl_3$ and HCHO took place within the dispersed aqueous droplets. The PtRu particles obtained from composition A were apparently smaller

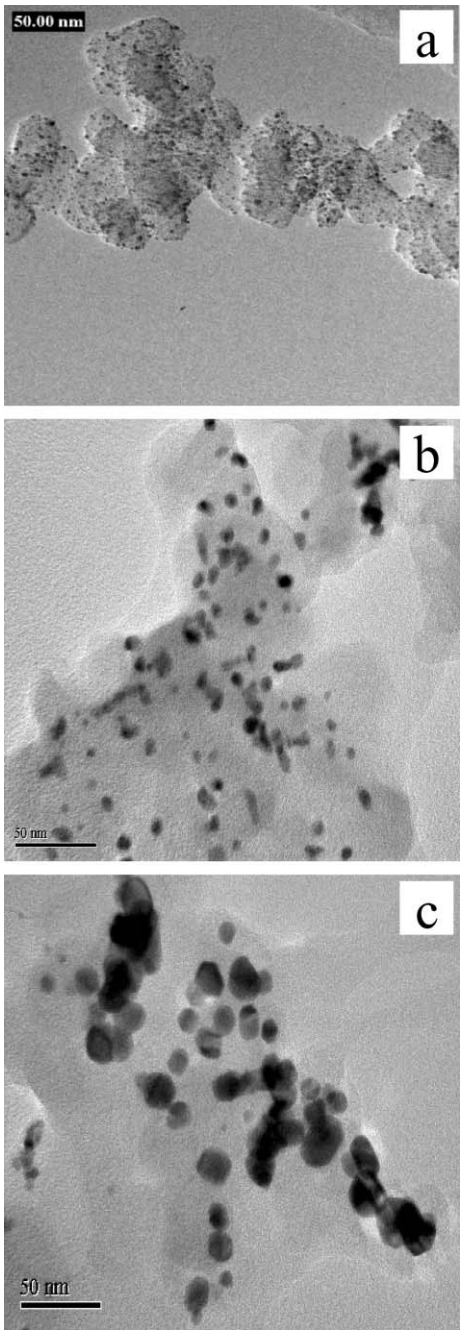

Fig. 3 Transmission electron micrographs of PtRu/C catalysts obtained from compositions: (a) A; (b) B; and (c) C.

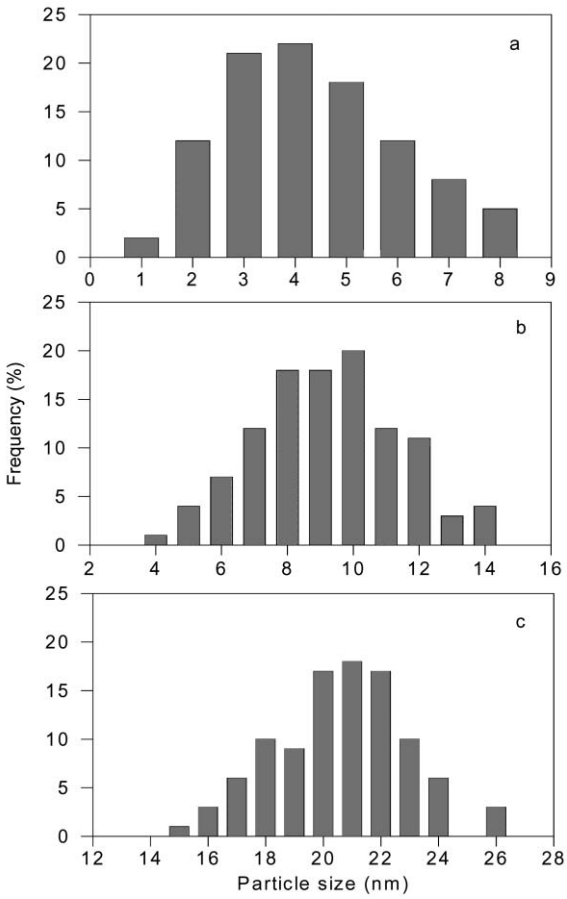

Fig. 4 Particle size distribution estimated from the TEM micrograph for the PtRu/C catalysts obtained from compositions: (a) A; (b) B; and (c) C.

than those from composition B due to a higher aqueous content in the latter. The reaction between H_2PtCl_6 or $RuCl_3$ and HCHO in larger aqueous domains would invariably lead to the

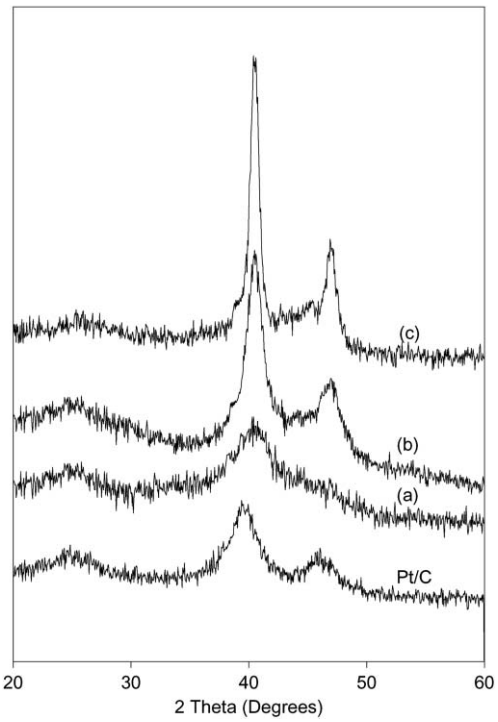

Fig. 5 XRD patterns for the PtRu/C catalysts obtained from compositions: (a) A; (b) B; and (c) C.

formation of large and more size-variable PtRu particles. The PtRu particles obtained from composition C, which was an o/w emulsion, were nanosize agglomerates typical of precipitation taking place in a continuous aqueous phase.

Fig. 4 shows the particle size distributions of the three PtRu/C catalysts, as measured by TEM. Average particle sizes of 4.3 $\pm$ 1.6 nm (based on 125 particles), 9.2 $\pm$ 2.1 nm (based on 87 particles) and 20.6 $\pm$ 2.2 nm (based on 118 particles) were obtained for PtRu/C catalysts from compositions A (transparent), B (translucent) and C (turbid emulsion), respectively.

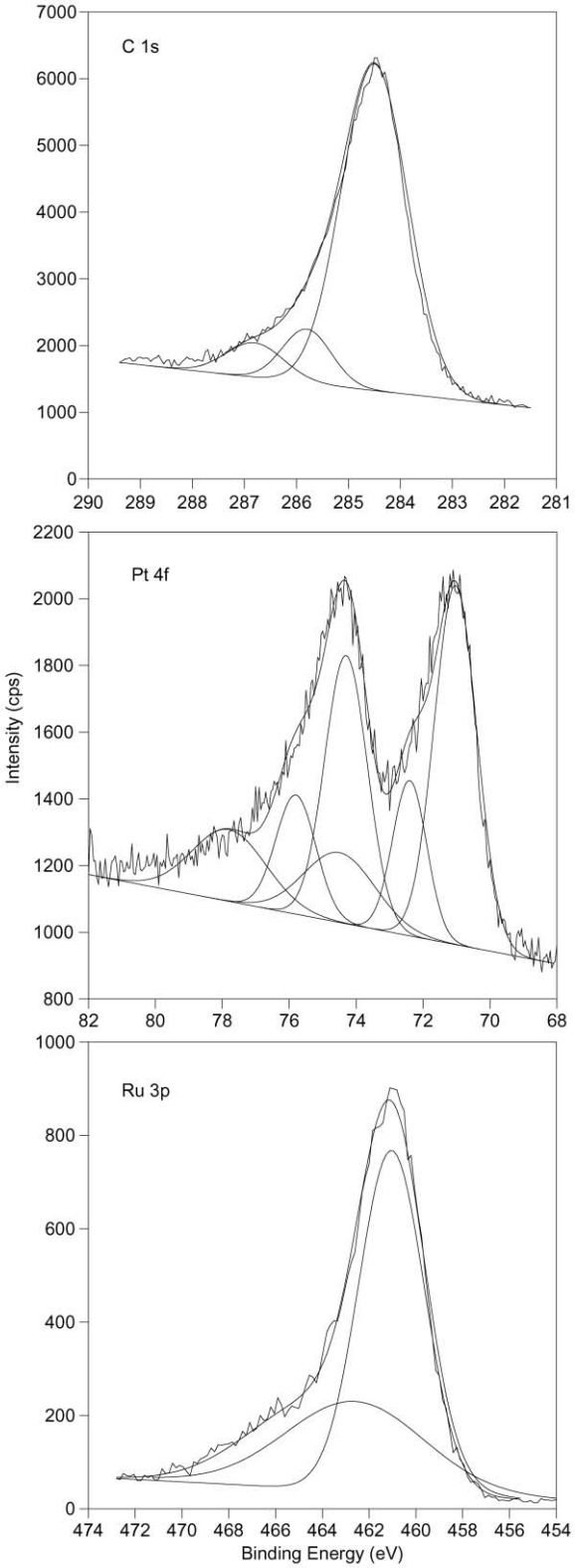

Fig. 6 X-ray photoelectron spectra of the PtRu/C catalyst obtained from composition A.

The PtRu particle size of the emulsion-derived catalyst was almost five times the size of particles from transparent (inverse) microemulsion preparation and twice the size of particles from translucent (inverse) microemulsion preparation. This is because the growth of precipitates formed in microemulsions was limited by the size of the reaction domains. As the aqueous droplets in an emulsion are generally bigger, particle growth was less hindered than in microemulsions, and large particles were formed. Among the various factors possibly affecting the catalytic activity of Pt–Ru alloy catalysts for methanol oxidation, the importance of particle size was recognized early. Higher intrinsic activity of the catalytic metal particles is common among ultrafine alloy particles which have a higher concentration of low-coordination surface metal atoms.[23] For an oxygen reduction electrocatalyst, the optimum particle size for a high mass activity was about 3 nm.[24] For methanol electrooxidation on carbon supported Pt–Ru catalysts, Takasu *et al.*[23] also measured the highest mass activity for the Pt_{50}–Ru_{50} catalyst at a size of about 3 nm.

The powder XRD patterns for the PtRu/C catalysts obtained from compositions A, B and C are shown in Fig. 5. For comparison, the diffraction pattern of a carbon-supported Pt catalyst has been included in Fig. 5. All PtRu electrocatalysts displayed the characteristic diffraction peaks of the Pt fcc structure, except that the 2θ values were shifted to slightly higher values. This is consistent with the observation of Chu and Gilman[25] who found that Pt–Ru alloys containing up to 52% Ru would show only Pt reflections with some shifts in the position of each diffraction peak. This is an indication of a solid solution formed at the atomic level with a basically unaltered fcc structure. Due to the ultrafine dimensions of the as-precipitated crystallites, there was extensive peak broadening in the XRD patterns for all three catalysts. Among them the catalyst from the o/w emulsion exhibited the highest crystallinity, as shown by sharp and more intense diffractions at $2\theta = 40.5^\circ$ and 47°. This corroborates the results of TEM examination where large particles predominated the emulsion preparation. X-ray scattering from the Vulcan carbon support was weak but was detectable around $2\theta = 25$–26°.

XPS was used to determine the surface oxidation states of the catalytic and co-catalytic metals. As most of the atoms in small particle clusters are surface atoms, the oxidation state measured as such would also reflect the bulk oxidation state. As the binding energy (BE) for the Ru 3d line of zero-valent ruthenium at 284.3 eV[26] is very close to the C 1s line resulting from adsorbed carbonaceous species, the Ru 3p spectrum was used instead for Ru oxidation state analysis. Fig. 6 shows the C

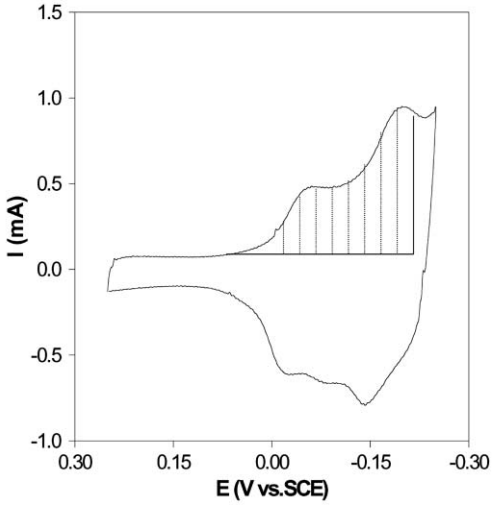

Fig. 7 Hydrogen electrosorption voltammetric profiles for the PtRu/C catalysts obtained from composition A. The hatched area represents the amount of charge of the electrosorption of hydrogen on Pt.

Table 1 The active surface area of PtRu catalysts as determined by hydrogen electroadsorption

Origin of PtRu/C catalyst	Q_H[a]/mC	Weight of catalyst/mg	A_{EL}[b]/m^2 g^{-1}	A_{TEM}[c]/m^2 g^{-1}	Onset potential/V	Peak i_{sp}/mA cm^{-2} PtRu
Composition A	11.2	0.45	11.9	13.0	0.19	0.24
Composition B	8.2	0.51	7.7	6.1	0.20	0.17
Composition C	4.3	0.50	4.1	2.7	0.22	0.05

[a]Charges exchanged during the electroadsorption of hydrogen atoms on Pt. [b]Pt surface obtained electrochemically. [c]Pt surface obtained from TEM.

1s, Pt 4f and Ru 3p regions of the XPS spectrum of the PtRu/C catalyst from composition A. The Pt 4f signal consisted of three pairs of Pt peaks. The most intense peaks (71.02 and 74.3 eV) were due to metallic Pt. The second set of doublets (72.4 and 75.2 eV), observed at BE 1.4 eV higher than Pt(0), could be assigned to the Pt(II) chemical state in PtO and $Pt(OH)_2$.[27] The third doublet of Pt peaks of weaker intensity, and at even higher BEs (74.5 and 77.8 eV), was most likely caused by a small amount of Pt(IV) species on the surface. The slight shift in the Pt(0) peak to higher binding energies is a known small particle size effect, as reported by Roth *et al.*[28] The C 1s spectrum appeared to be composed of graphitic carbon (284.6 eV) and –C=O like species (285.83 eV).[27] A small amount of surface functional groups with higher oxygen content was noted in the spectrum (BE 286.8 eV). The large C 1s spectrum from the carbon support at about 284.6 eV overlapped with the Ru $3d_{3/2}$ peak (284 eV) preventing an accurate determination of the Ru oxidation state at this BE value. Nevertheless the peak at 280.5 eV in the tail of the large C 1s peak could be attributed to zero-valent Ru.[29] The Ru $3p_{3/2}$ signal was deconvoluted into two distinguishable pairs of peaks of different intensities at BE = 461.1 and 462.7 eV, corresponding to Ru(0) and RuO_2, respectively.[30]

Electrochemically active surface areas for the PtRu/C powders could be estimated from the integrated charge in the hydrogen absorption region of the cyclic voltammogram (hatched area in Fig. 7). The surface areas in m^2 g^{-1} were calculated from the following formula assuming a correlation value of 0.21 mC cm^{-2} (calculated from a surface density of 1.3×10^{15} atom cm^{-2}, a value generally admitted for polycrystalline Pt electrodes[31]) and the Pt loading.

$$A_{EL}\ (\mathrm{m^2\ g^{-1}\ Pt}) = Q_H/(0.21 \times 10^{-3}\mathrm{C} \times \text{amount of catalyst})$$

where A_{EL} is the Pt surface obtained electrochemically, Q_H is the amount of charge exchanged during the electroadsorption of hydrogen atoms on Pt and C is Coulomb.

From the calculation results in Table 1, the PtRu catalyst obtained from composition A has the highest active surface area. This is not surprising in view of the small particle size of this catalyst.

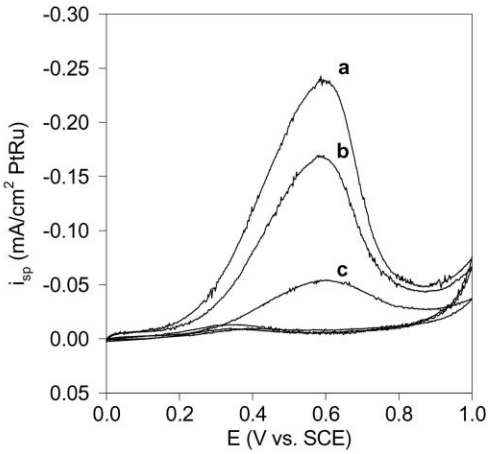

Fig. 8 Cyclic voltammograms for PtRu/C electrodes in Ar-saturated 1 M H_2SO_4 with 2 M methanol present in the electrolyte at 10 mV s^{-1}. PtRu/C catalysts prepared from compositions: (a) A; (b) B; and (c) C.

The cyclic voltammograms for methanol oxidation on these PtRu/C catalysts are compared in Fig. 8, using potential sweeps between 0 and 1.0 V. In the anodic scan, methanol oxidation produced a large anodic peak at 0.6 V and was the most prominent for the PtRu/C catalyst from composition A. The electrochemical activity, as ranked by the intensity of the 0.6V peak, follows the order from A to C. The order agreed well with the difference in electrochemical specific surface area and average particle size. Table 1 shows the active surface areas increases from 4.1, to 7.7 and 11.9 m^2 g^{-1} from compositions C to B to A, while the increase in peak current follows a similar trend, an exact proportionality relationship between peak current density and specific surface area was not obtained.

In experiments on methanol oxidation, current density above the background level was detected as early as 0.1 V, and began to escalate rapidly at 0.2 V. This may be interpreted in terms of a water discharge reaction producing OH species that were chemisorbed on the Ru sites. The anodic overpotential for the water discharge reaction on Ru sites and the formation of surface Ru–OH groups is lower than that on Pt sites. It is the general belief that the Pt sites in a Pt–Ru alloy are involved in particular in both the methanol dehydrogenation step and in the strong chemisorption of methanol residues. At 0.2 V, the water discharge reaction occurs mostly on the Ru sites of the catalyst surface. The final step is a reaction between the Ru–OH groups and neighbouring methanolic residues on Pt to yield carbon dioxide.

Conclusions

Nanosize PtRu alloy particles on carbon support were prepared by microemulsion based techniques, using H_2PtCl_6 (0.025 M)/$RuCl_3$ (0.025 M)/NaOH (0.025 M) as the aqueous phase, cyclohexane as the oil phase and NP5 + NP9 as the surfactant. PtRu particles of between 4 and 9 nm could be obtained from transparent and translucent inverse microemulsions. All catalysts prepared as such have shown characteristic diffraction peaks pertaining to the Pt fcc structure. XPS analysis revealed that the catalysts contained mostly Pt(0) and Ru(0), with a little Pt(II), Pt(IV) and Ru(IV). The two microemulsion-derived PtRu/C catalysts had high electrocatalytic activities for methanol oxidation over that of the emulsion-derived PtRu/C electrocatalyst. The peak current density for methanol oxidation at PtRu/C obtained from the transparent inverse microemulsion was about four times that of the emulsion-derived PtRu/C.

References

1 C. S. Cameron, G. A. Hards and D. Thompsett, *Proc. - Electrochem. Soc.*, 1992, **92-14**, 10.
2 X. Ren, M. S. Wilson and S. Gottesfeld, *J. Electrochem. Soc.*, 1996, **143**, L12.
3 S. Wasmus and W. Vielstich, *J. Appl. Electrochem.*, 1993, **23**, 120.
4 H.–F. Oetjen, V. M. Schmidt, U. Stimming and F. Trila, *J. Electrochem. Soc.*, 1996, **143**, 3838.

5 R. A. Lemons, *J. Power Sources*, 1990, **29**, 251.
6 H. A. Gasteiger, N. Markovic, P. N. Ross and E. J. Cairns, *J. Phys. Chem.*, 1994, **98**, 617.
7 H. A. Gasteiger, N. Markovic and P. N. Ross, *J. Phys. Chem.*, 1995, **99**, 8290.
8 A. Giroir-Fendler, D. Richard and P. Gallezot, *Faraday Discuss.*, 1991, **92**, 69.
9 M. Watanabe, M. Uchida and S. Motoo, *J. Electroanal. Chem.*, 1987, **229**, 395.
10 T. J. Schmidt, M. Noeske, H. A. Gasteiger and R. J. Behm, *J. Electrochem. Soc.*, 1998, **145**, 925.
11 H. Bönnemann, R. Brinkmann, P. Britz, U. Endruschat, R. Mörtel, U. A. Paulus, G. J. Feldmeyer, T. J. Schmidt, H. A. Gasteiger and R. J. Behm, *J. New Mater. Electrochem. Syst.*, 2000, **3**, 199.
12 E. M. Crabb, R. Marshall and D. Thompsett, *J. Electrochem. Soc.*, 2000, **147**, 4440–4447.
13 M. Götz and H. Wendt, *Electrochim. Acta*, 1998, **43**, 3637.
14 E. Scolan and C. Sanchez, *Chem. Mater.*, 1998, **10**, 3217.
15 P. K. Sharma, M. H. Jilavi, D. Burgard, R. Nass and H. Schmidt, *J. Am. Ceram. Soc.*, 1998, **81**, 2732.
16 M. P. Pileni, *Cryst. Res. Technol.*, 1998, **33**, 1155.
17 D. C. Blackley, in *Polymer Latices*, Chapman and Hall, London, 2nd edn., 1997.
18 K. Landfester, *Adv. Mater.*, 2001, **13**, 765.
19 B. K. Palu and S. P. Moulike, *J. Dispersion Sci. Technol.*, 1997, **18**, 301.
20 L. M. Gan and C. H. Chew, in *Advanced Functional Molecules and Polymers*, ed. H. S. Nalwa, Gordon and Breach, New York, 1999.
21 D. Langevin, *Acc. Chem. Res.*, 1988, **21**, 257.
22 G. K. Lim, J. Wang, S. C. Ng, C. H. Chew and L. M. Gan, *Biomaterials*, 1997, **18**, 1433–1439.
23 Y. Takasu, H. Itaya, T. Iwazaki, R. Miyoshi, T. Ohnuma, W. Sugimoto and Y. Murakami, *Chem. Commun.*, 2001, 341–342.
24 N. Giordano, E. Passalacqua, L. Pino, A. S. Aricò, V. Antonucci, M. Vivaldi and K. Kinoshita, *Electrochimica Acta*, 1991, **36**, 1979.
25 D. Chu and S. Gilman, *J. Electrochem. Soc.*, 1996, **143**, 1685.
26 J. F. Moulder, W. F. Stickle, P. E. Sobol and K. D. Bomben, in *Handbook of X-ray Photoelectron Spectroscopy*, Perkin-Elmer, Eden Prairie, MN, 1992.
27 A. K. Shukla, M. K. Ravikumar, A. Roy, S. R. Barman, D. D. Sarma, A. S. Aricò, V. Antonucci, I. Pino and N. Giordano, *J. Electrochem. Soc.*, 1994, **141**, 1517.
28 C. Roth, M. Goetz and H. Fuess, *J. Appl. Electrochem.*, 2001, **31**, 793.
29 C. D. Wagner, W. M. Riggs, L. E. Davis and J. F. Moulder, in *Handbook of X-Ray Photoelectron Spectroscopy*, ed. G. E. Mullemberg, Perkin-Elmer, Eden Prairie, MN, 1978.
30 R. Kötz, H. J. Lewerenz and S. Stucki, *J. Electrochem. Soc.*, 1983, **130**, 825.
31 R. Woods, *J. Electroanal. Chem.*, 1976, **9**, 1.